EURASIAN JOURNAL OF MATHEMATICAL AND COMPUTER APPLICATIONS
ISSN 2306–6172
Volume 14, Issue 1 (2026) 43 – 58

MODELING OF THE LIQUID COOLING SYSTEM FOR HIGH-POWER ELEMENTS OF TECHNICAL MEANS

Piskun G. A. * , **Alekseev V. F.**, **Pavlovets N. A.**

Abstract The article evaluates the efficiency of a liquid cooling system designed for high-power components of modern computing systems, including the central processing unit (CPU), memory chips, and graphics processing unit (GPU). To achieve this, a detailed three-dimensional model of a personal stationary computer was developed using the Solid Edge (Siemens) software environment. The study employed the FloEFD (Flow Simulation) module to simulate hydrodynamics and heat transfer processes, enabling accurate analysis of thermal performance. Key parameters such as ambient temperature (ranging from 263 K (-10 °C) to 313 K (40 °C)), type of refrigerant (water (H2O), EK-CryoFuel, and Koolance LIQ-702), and the number of operational fans (one to three) were systematically investigated to determine their impact on cooling efficiency. The results provide insights into optimizing liquid cooling systems under varying environmental and operational conditions, offering valuable guidance for improving thermal management in high-performance computing environments. This research highlights the importance of considering multiple factors when designing efficient cooling solutions for advanced technical systems.

Key words: heat transfer, central processing unit, memory chips, graphics processing unit, refrigerant, FloEFD, hydrodynamics, liquid cooling system, computer simulation, microchannels, Solid Edge.

AMS Mathematics Subject Classification: 76D05, 80M10, 76F60, 80A20.

DOI: 10.32523/2306-6172-2026-14-1-43-58

1 Introduction

High-performance computing equipment contains heat-generating components such as the central processing unit (CPU), graphics processing unit (GPU), memory chips, and others. Effective cooling systems are essential to ensure uninterrupted operation and optimal performance by preventing overheating of these elements.

Air and liquid cooling principles form the basis for building efficient heat removal systems. Each approach has its advantages and disadvantages. In particular, liquid cooling systems (LCS) generally outperform air cooling systems in terms of efficiency and performance [1–3]. This superiority arises from the higher thermal conductivity of liquid coolants compared to air and their ability to maintain a more uniform temperature distribution throughout the system.

The present study investigates the application of an LCS to maintain optimal temperatures of the motherboard's central processing unit, memory chips, and graphics processing unit of the graphics card. It examines the dependence of LCS efficiency on ambient temperature, coolant type, and the number of fans in the radiator system.

To determine the optimal parameters of the LCS, a three-dimensional computational model

of a stationary personal computer was developed in the Solid Edge (Siemens) software environment. The FloEFD (Flow Simulation) module was used for testing and calculations, as it enables the solution of complex problems involving coupled thermal processes and fluid flow.

2 Development of an LCS Simulation Model

Liquid cooling systems for modern stationary technical equipment typically include a water block for the processor (1) and graphics card (2), the device case (3), connecting tubes (hoses) (4), a radiator (5) with an installed fan system (6), and a pump (7) (Fig. 1).

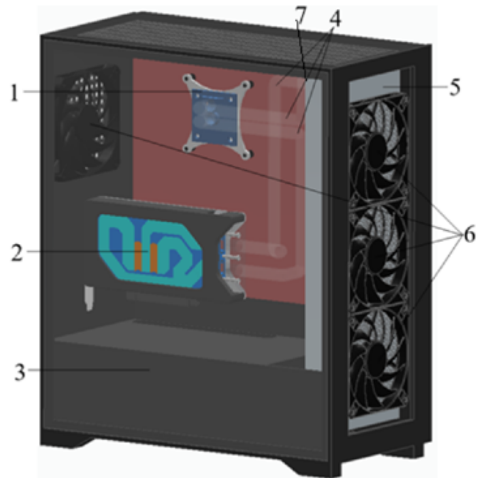

Figure 1: Three-dimensional model of a perforated personal computer case with liquid cooling system.

A personal computer case with dimensions 200×400×470 mm and a large number of perforated holes was selected as the model. The perforations ensure the inflow of cold air and the outflow of hot air. The case material is stainless steel, and one side panel is made of glass.

2.1 Processor Water Block Model

The Intel Core i9-13900K [4] CPU was selected for the study. It is regarded as one of the highest-performance processors available for stationary computers. With a power consumption of 253 W, it exhibits significant heat dissipation, making it suitable for evaluating LCS efficiency.

The EK-CPU Lignum – Walnut [5] water block was adopted as the model (Fig. 2). It features a simple design in which the coolant enters the heat sink through the inlet (perpendicular to the processor), increasing fluid velocity. The coolant is then distributed through microchannels across the water block and exits perpendicularly to the processor via the outlet.

The water block consists of a cover, mounting bracket, and heat sink. The heat sink is made of copper, while the mounting bracket and cover are made of aluminum. A 0.08 mm layer of thermal paste (thermal conductivity 4 W/(m·K)) is applied between the processor and the heat sink to fill gaps and improve heat dissipation.

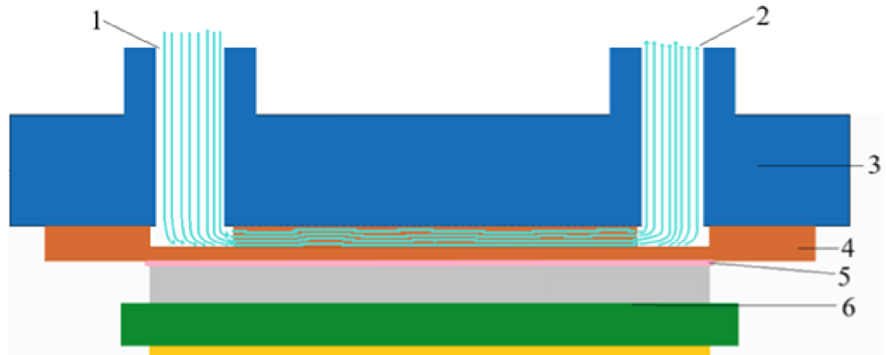

Figure 2: Design of the processor water block. 1 - inlet, 2 - outlet, 3 - cover, 4 - heat sink, 5 - thermal paste, 6 - processor

2.2 Video Card Water Block Model

The NVIDIA GeForce RTX 3090 Founders Edition [6] graphics card was selected for the study. It includes high-heat-flux components such as the GeForce RTX 3090 GPU (maximum frequency 1830 MHz) and GDDR6X memory chips (power consumption 2.5–3.0 W each).
The EK-Quantum Vector FE RTX 3090 D-RGB – Black Special Edition [7] water block, equipped with a massive heat sink, was used as the model. An additional aluminum plate dissipates heat from less heat-intensive elements without involving the main heat sink (Fig. 3). The coolant enters the water block through the inlet, flows through a channel into the distribution plate, passes through a narrow gap, and moves along the microchannels of the heat sink, removing heat from the graphics card components via a layer of thermal paste. The coolant then spreads across the block, extracting heat from the heat sink, and exits through dedicated channels.

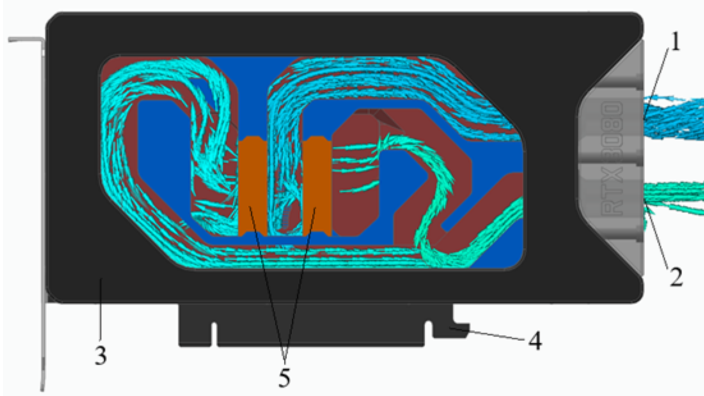

Figure 3: Trajectory of fluid movement inside the video card water block. 1 - inlet, 2 - outlet, 3 - water block, 4 - board, 5 - aluminum heat sinks

The refrigerant enters the video card water block through the inlet, where, flowing through the channel, it enters the distribution plate. Through a narrow gap in the plate, it moves along the microchannels of the heat sink, which remove heat from the video card components through a layer of thermal paste. Then the refrigerant is distributed across the water block,

simultaneously removing heat from the heat sink. After that, the liquid flows through special channels and exits the water block. This model has the following characteristics:
-heat sink material – copper;
-printed circuit board material – fiberglass;
-pousing materials – polyamide, glass;
-GPU power – 200 W;
-heat dissipation power of other elements was set at the maximum level, resulting in total power consumption of the entire graphic card being 350 W;
-properties of additional layers not accounted for in the model: thickness of the thermal paste layer between GPU and heat sink – 0.05 mm; thickness of thermal pads between remaining high-power elements and heat sink – 1 mm; thermal conductivity coefficient of thermal paste – 4 W/(m·K).

2.3 Radiator Model with Installed Fan System

The EK-CoolStream Classic PE 360 [8] radiator was selected as the model (Fig. 4). This model is the most common in similar LCSs, and its heat dissipation capabilities are sufficient for this project.

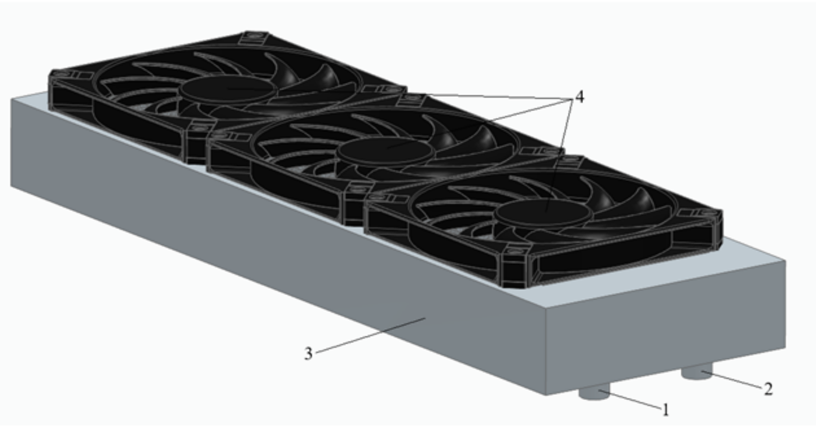

Figure 4: Model of the EK-CoolStream Classic PE 360 radiator. 1 - inlet, 2 - outlet, 3 - radiator, 4 - fans

This radiator with dimensions 405×130×40 mm is made of aluminum, consists of an outer casing, 14 heat pipes with a diameter of 2.0 mm, heat-dissipating fins with a width of 5.6 mm and a thickness of 0.2 mm. During the development of the radiator model, three fans were used located on the front panel of the case. They provide effective radiator airflow and allowing to reduce the refrigerant temperature.
A fan is installed on the back part of the mock-up, which removes hot air from the case. Such placement of fans on the case is the most common since it contributes to effective air circulation inside it.
The Corsair AF120 SLIM [9] fan was selected as the model, which has a small size while maintaining all technical characteristics. The fan material is polyamide, their rotation speed is 2000 rpm.

2.4 Pump and Connecting Tubes Model

The EK-Quantum Kinetic³ FLT 92 D5 PWM D-RGB – Plexi [10] water cooling pump was selected as the model. It has small dimensions and its capacity will be sufficient to maintain a stable refrigerant flow in the system. In particular, the maximum volumetric flow rate is 1000 l/h, the maximum created pressure difference is 50912 Pa, the rotation speed is 2000 rpm.
When using the pump, a turbulent flow of increased pressure forms at its outlet, and decreased pressure at its inlet (Fig. 5). Connecting tubes (hoses) made of polybutylene terephthalate (PBT) with a diameter of 15 mm were added to move the refrigerant from one system component to another.

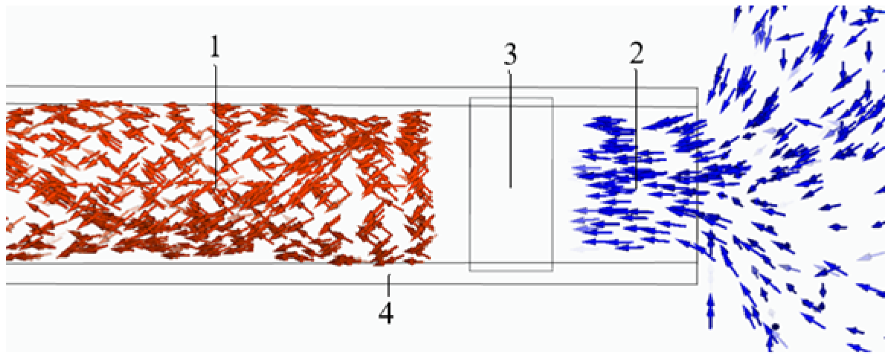

Figure 5: Pressure increase of the refrigerant by the pump. 1 - high-pressure area, 2 - low-pressure area, 3 - pump, 4 - PBT tube

3 Mathematical Formulas for Analyzing the Liquid Cooling System

The most effective physical-mathematical model for describing heat transfer in LCS is a system of equations including:
- Navier-Stokes equation, which describes the motion of viscous incompressible fluid (refrigerant density change does not exceed 4 percent) and shows that the change in fluid flow velocity depends on pressure gradient, viscosity, and gravity [11]:

$$\rho\left(\frac{\partial U}{\partial t} + (U \cdot \nabla)U\right) = -\nabla P + \mu\nabla^2 U + \rho g \tag{1}$$

where ρ - fluid density (kg/m), U – fluid flow velocity (m/s), t – time (s), ∇ – nabla operator, p – pressure (Pa), μ – medium shear viscosity (Pa· s), ρg – volume force (N/m^3);

- continuity equation, necessary to describe and analyze the fluid motion in the circuit, shows the relationship between the density change and the velocity of fluid flow and the pressure change [11]:

$$\frac{\partial \rho}{\partial t} + \nabla \cdot (\rho U) = 0 \tag{2}$$

where $\nabla \cdot (\rho U)$ – divergence operator, which calculates the change in refrigerant mass flow through a unit area;
- heat conduction equation, which describes the heat transfer process in the refrigerant and accounts for both temporal temperature changes and spatial gradients [11, 12]:

$$\rho Cp \frac{\partial T}{\partial t} + \rho C(U \cdot \nabla)T = \lambda \nabla^2 T \tag{3}$$

where $Cp = Cp(T)$ – isobaric specific heat capacity, T - temperature (K), $\lambda = \lambda(T)$ - thermal conductivity coefficient, $\nabla^2 \cdot T$ - temperature gradient.
In the left part of equation (3), changes in the internal energy of the system over time ($\rho C_p \frac{\partial T}{\partial t}$) and temperature due to convective heat transfer with the moving fluid ($\rho C(U \cdot \nabla)T$) are described. From the right part of the equation, it can be seen that if the thermal conductivity coefficient is constant, then $\nabla(\lambda \nabla T) = 0$. However, in the studied LCS design, there are several heat sources with different temperature values.
- equation related to creating the refrigerant velocity flow due to using the pump [13]:

$$\Delta p(g) = \frac{8g^2}{\pi^2 d_e^4 \rho} + \frac{114Lg}{\pi d_e^4 \rho \mu} \tag{4}$$

where Δp – pressure drop (Pa), g – fluid mass flow rate (kg/s), d_e – equivalent pipe diameter (m), L – hose length (m).
The feature of formula (4) is that it describes two main ways of pressure loss in the hose: due to friction and due to viscosity. The first term $(8g^2/(\pi^2 de^4 \rho))$ shows that the loss depends on the mass flow rate, density, and hose diameter. The higher the flow velocity, the greater the pressure loss due to friction will be. The second term of the equation $(114Lg\mu/(\pi^2 de^4 \rho))$ shows how fluid viscosity affects flow resistance, i.e., the longer the hose, the greater the pressure loss will be.

4 Numerical Methodology and Model Verification

The fundamental stage of this work is the construction of an adequate mathematical model capable of high-precision reproduction of the complex processes of conjugate heat transfer and turbulent hydrodynamics occurring within the chassis of a high-performance computing system [14-18]. To implement this task, the FloEFD software package was chosen, which integrates computational fluid dynamics (CFD) methods directly into the computer-aided design environment, thereby avoiding geometric accuracy losses during object import. The software's computational core is based on the numerical solution of the Reynolds-Averaged Navier-Stokes (RANS) equations [19-22]. As a mathematical basis for describing turbulence effects, a modified two-parameter $k - \omega$ SST model was applied in the study.

4.1 Mathematical Model and Convergence Criteria

As a mathematical basis for describing turbulence effects, a modified two-parameter $k-\omega$ SST model was applied in the study [19-21]. Unlike standard isotropic models, the implementation in the software package used includes unique enhanced wall functions that allow for correct calculation of boundary layer parameters even under complex channel topologies. This is achieved through a combined approach that integrates analytical solutions for the viscous sublayer and numerical methods for the outer part of the turbulent boundary layer, minimizing

mesh density requirements near solid bodies. Particular attention was paid to ensuring strict numerical solution convergence. The iterative process continued until the root-mean-square residuals for all primary conservation equations reached a level of 10^{-5}, which is a generally accepted industrial standard for high-precision engineering calculations. Furthermore, integral goal parameters, such as the maximum surface temperature of the silicon crystals of central and graphics processors, were used as additional convergence indicators. The calculation was considered complete only after the amplitude of these temperature fluctuations did not exceed 0.1 K over the last hundred iterations. All computations were performed in a steady-state formulation aimed at finding the steady thermal balance of the system under maximum operating loads.

4.2 Boundary Conditions

The determination of boundary conditions was based on detailed technical specifications of real electronic components operating in maximum heat dissipation mode. The Intel Core i9-13900K central processing unit was modeled as a volumetric heat power source of 253 W, corresponding to its peak Turbo mode power limit. For the NVIDIA GeForce RTX 3090 graphics adapter, a fixed heat dissipation power of 350 W was established. The model accounted for the multi-layer heat transfer structure, including copper heat spreaders and thin thermal interface layers with a thermal conductivity of 8.5 W/(m·K). Distilled water with a volume flow rate of 1.5 liters per minute was considered as the refrigerant in the baseline scenario, corresponding to the performance of a typical D5 standard pump at medium speeds. The initial coolant temperature at the loop inlet was fixed at 293.15 K, while a static atmospheric pressure condition was set at the system outlets. The hydraulic resistance of all connecting fittings, hoses, and the radiator was calculated automatically based on their real geometry and wall roughness, providing a reliable picture of the pressure drop in the closed loop.

4.3 Grid Independence Study and Domain Discretization

The construction of the computational mesh was a hierarchical procedure aimed at minimizing discretization errors while maintaining computational efficiency. An adaptive rectangular Cartesian mesh with octree refinement and SIMPLE[22] technology was utilized. This technology allows a single computational cell to contain multiple control volumes, which is critical for correctly describing heat transfer at the fluid-solid interface. To ensure high accuracy in intense heat transfer zones, such as water block microchannel structures with a fin pitch of less than 0.5 mm, local mesh refinement up to the fifth adaptation level was applied. This achieved a resolution of 6–10 computational cells across each channel, necessary for accurately determining temperature and velocity gradients in the viscous sublayer of the coolant. For quantitative accuracy assessment and model validation, a grid independence test was conducted, the results of which are summarized in the table below. The comparative analysis of the data in the table shows that the initial coarse calculation significantly overestimated the temperature, due to the inability of the sparse mesh to adequately describe the flow structure. An ultra-detailed mesh of 5 million cells showed a temperature change of only 0.5 percent relative to the baseline. Such a minor refinement despite a manifold increase in computation time confirms the achievement of asymptotic independence of the solution from mesh parameters, making the 1-million-cell baseline optimal for all subsequent serial calculations.

Table 1: Impact analysis of computational mesh density on calculation accuracy

Mesh Configuration	Total Cells	CPU Temperature (max), K	Relative Error, percent
Coarse Mesh	$300,000$	345.6	+4.0
Baseline Mesh	$1,000,000$	332.3	Reference
Fine Mesh	$5,000,000$	330.6	$\mid -0.5$

4.4 Optimization Approach

The final element of the methodology was a multi-parameter optimization analysis aimed at identifying the best cooling system configuration [24-28]. Instead of a simple comparison of options, the work investigated the complex relationship between the thermodynamic properties of various refrigerants and heat removal efficiency under different radiator fan operating modes. The optimization aimed to minimize the overall thermal resistance of the system while adhering to a strict temperature limit of 373 K, beyond which thermal throttling mechanisms are activated. The impact of transitioning from standard water to EK-CryoFuel and Koolance LIQ-702 type refrigerants was investigated, as well as the change in airflow intensity through the radiator by varying the number of active fans from one to three. The data obtained revealed thermal efficiency saturation points, beyond which a further increase in flow velocity or fan power does not lead to a significant temperature reduction, which is crucial for balancing cooling performance and the acoustic comfort of the system.

5 Experiments to Evaluate LCS Efficiency

After creating and preparing all the models, the LCS and its parameters were checked for adequacy. For this purpose, model parameters were set with the following characteristics: ambient temperature – 20 °C; refrigerant – H2O; number of working fans – 3 pcs.; TDP of the processor and video card elements, pump volumetric flow rate, fan rotation speed – maximum possible values.

To simplify the analysis calculation, control points were set – sections of the model from which temperature readings were taken, namely: central processing unit temperature (CPU); temperatures at the inlet (CPU enter) and outlet (CPU exit) of the processor water block; graphics processing unit temperature (GPU); temperatures at the inlet (GPU enter) and outlet (GPU exit) of the video card water block; temperature on the video memory chips (Memory); temperatures at the inlet (Radiator enter) and outlet (Radiator exit) of the radiator.

After performing the mock-up calculation, a graph of the dynamics of refrigerant temperature change as it moves through the LCS was constructed (Fig. 6), vectors of air movement (Fig. 7) and refrigerant (Fig. 8) inside the device case were graphically marked.

The temperature values of the mock-up heat-loaded elements are shown in Table 1.

Table 2: Temperature values of the mock-up heat-loaded elements

heat-loaded element	**CPU**	**GPU**	**Memory**
Temperature T, K	332,3	336,3	330,7

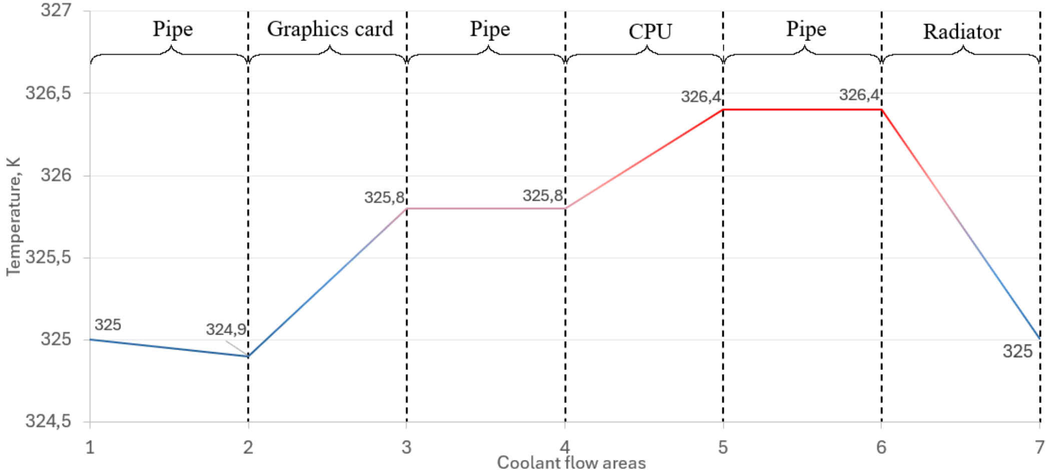

Figure 6: Dynamics of refrigerant temperature change considering various LCS areas

Based on the simulation results, the obtained temperature values were compared with those of a real model: the obtained values turned out to be lower than the real ones, which is associated with setting the maximum possible system parameters, slight differences in design, and unknown ambient temperature values in the real model. Therefore, based on the comparison, it can be concluded that the proposed model is quite accurate, and further studies of dependencies described above can be continued based on it. All obtained values of the reference model will be used for comparison and analysis of the described dependencies in the future.

5.1 Influence of Ambient Temperature on LCS Efficiency

To check the dependence of system component temperatures on ambient temperature, calculations were performed where the ambient temperature varied in the range from 263 K (-10 °C) to 313 K (40 °C) with a step of 10 K. The temperature values of heat-loaded elements and temperatures at different system points at various ambient temperatures are shown in Tables 3 and 4, respectively.

Table 3: Temperature values of heat-loaded elements at various ambient temperatures

Ambient temperature, K	**Temperature, K, of heat-loaded element**		
	CPU	**GPU**	**Memory**
263	308.6	312.7	307.0
273	316.7	320.7	315.1
283	329.7	333.6	328.0
293	332.3	336.3	330.7
303	345.2	349.0	343.7
313	352.0	355.9	350.7

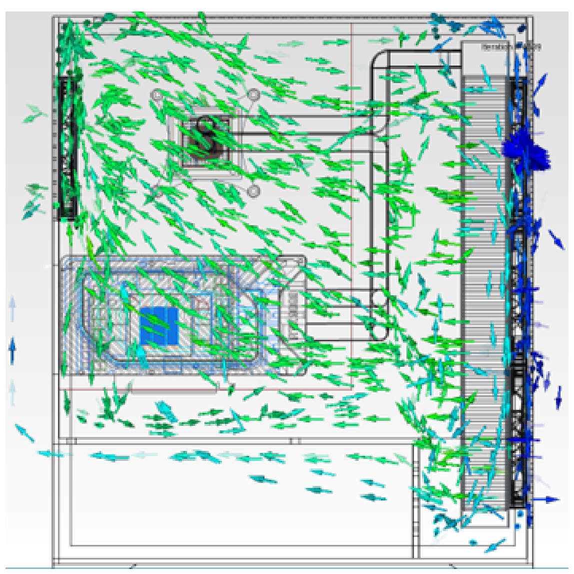

Figure 7: Vectors of air movement inside the device case

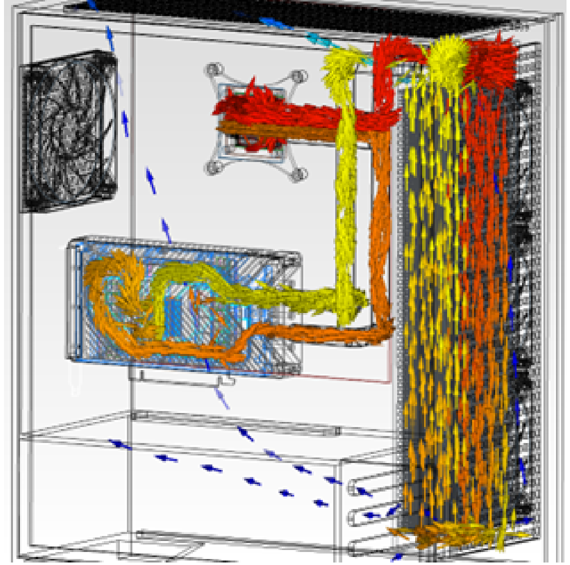

Figure 8: Vectors of refrigerant movement and its temperature distribution inside the device case

Table 4: Temperature values at different system points at various ambient temperatures

Ambient temperature, K	**Temperature, K, at system point**					
	CPU enter	**CPU exit**	**GPU enter**	**GPU exit**	**Radiator enter**	**Radiator exit**
263	300.7	303.3	301.7	301.7	302.4	300.8
273	310.0	310.7	309.1	310.0	310.6	309.1
283	323.1	323.8	322.2	323.2	323.8	322.3
293	325.8	326.4	324.9	325.8	326.4	325.0
303	338.9	339.5	338.0	338.9	339.5	338.1
313	345.9	346.6	345.1	346.0	346.5	345.1

5.2 Influence of Refrigerant on LCS Efficiency

To check the dependence of component temperatures on the used refrigerant, calculations were performed where H2O was replaced with EK-CryoFuel and Koolance LIQ-702. These refrigerants can be used for electronic equipment cooling. Technical characteristics of the refrigerants are presented in Table 5.

The temperature values of heat-loaded elements and at different system points when using various refrigerants are shown in Tables 6 and 7, respectively.

Table 5: Technical characteristics of refrigerants

Refrigerant characteristic	**Distilled water (H2O)**	**EK-CryoFuel**	**Koolance LIQ-702**
Dynamic viscosity, Pa·s	$1.002 \cdot 10^{-3}$	$(0.2 - 0.3) \cdot 10^{-3}$	$(0.15{-}0.20)\cdot 10^{-3}$
Thermal conductivity, W/(m·K)	0.598	0.07–0.08	0.013–0.015
Boiling temperature, K	373.15	300.15	247.15

Table 6: Temperature values of heat-loaded elements when using various refrigerants

Type of refrigerant	**Temperature, K, of heat-loaded element**		
	CPU	**GPU**	**Memory**
H2O	332.3	336.3	330.7
EK-CryoFuel	347.9	351.6	342.4
Koolance LIQ-702	343.8	348.0	339.9

The analysis of the simulation results shows that the choice of distilled water as a refrigerant is the most justified from the perspective of the heat transfer physics described by equation (3). The main contribution to the cooling efficiency is made by two terms of this equation: the convective term $c_p(\mathbf{u} \cdot \nabla T)$ and the diffusion term $\nabla \cdot (\lambda \nabla T)$.
A comparative analysis of the thermophysical properties of the refrigerants at an operating temperature of 300 K allows for a quantitative estimation of the heat flux density q according to Fourier's law, which underlies the diffusion part of equation (3) [23]:

$$q = -\lambda \nabla T \tag{5}$$

For water, the thermal conductivity coefficient is $\lambda_{H2O} \approx 0.608$ W/(m·K), while for Freon EK-CryoFuel it is $\lambda_{EK-CryoFuel} \approx 0.071$ W/(m·K). With the same temperature gradient ∇T at the "water block wall — liquid" interface, the ratio of heat transfer efficiencies is [15]:

$$\frac{q_{H2O}}{q_{EK-CryoFuel}} = \frac{\lambda_{H2O}}{\lambda_{EK-CryoFuel}} = \frac{0.608}{0.071} \approx 8.56 \tag{6}$$

This means that water is capable of removing heat from the copper base of the water block 8.5 times more intensively than EK-CryoFuel. This explains the temperature difference recorded in the experiment: for the Intel Core i9-13900K processor, the temperature when using water was 328.7 K, whereas when using EK-CryoFuel, it increased to 344.3 K ($\Delta T = 15.6$ K).
Furthermore, the left side of equation (3) accounts for the thermal inertia of the flow through the product ρc_p. The specific heat capacity of water $c_{p,H2O} \approx 4180$ J/(kg·K) significantly exceeds that of Freons ($c_{p,EK-CryoFuel} \approx 1000$ J/(kg·K)). Substituting these values into the power balance equation $Q = \dot{m} c_p \Delta T_{fluid}$, we see that to absorb a thermal power of $Q \approx 600$ W (total CPU and GPU load) at the same mass flow rate $\dot{m}$, Freon must heat up 4.1 times more than water. This inevitably leads to an increase in the average temperature of the system

Table 7: Temperature values at different system points when using various refrigerants

Type of refrig- erant	**Temperature, K, at system point**					
	CPU enter	**CPU exit**	**GPU enter**	**GPU exit**	**Radiator enter**	**Radiator exit**
H2O	325.8	326.4	324.9	325.8	326.4	325.0
EK-CryoFuel	334.1	336.0	331.7	334.3	335.9	331.8
Koolance LIQ-702	332.9	334.5	330.9	333.0	334.4	330.9

and a decrease in the efficiency of heat exchange at the radiator, which is confirmed by the temperature distributions obtained in Figure 6. Thus, the application of the mathematical model allowed us to confirm that the high heat capacity and thermal conductivity of water offset its higher density ρ, minimizing the impact of pressure losses Δp from equation (4).

5.3 Influence of Number of Working Fans on LCS Efficiency

To examen the dependence of system components temperature on the number of working fans, the specific calculations was performed: starting from the bottom, one fan was sequentially turned off on the front panel of the case. Tables 8 and 9 represent the temperature values of heat-loaded components and temperature at different system points, respectively, at different numbers of operating fans.

Table 8: Temperature values of heat-loaded elements at various numbers of working fans

Number of fans, pcs.	**Temperature, K, of heat-loaded element**		
	CPU	**GPU**	**Memory**
3	332.3	336.3	330.7
2	337.7	341.6	336.1
1	358.2	362.4	357.1

The physical interpretation of the dependence of cooling efficiency on the number of operating fans is based on the analysis of the convective term $c_p(\mathbf{u} \cdot \nabla T)$ in the energy equation (3). The air flow velocity $\mathbf{u}$ directly determines the intensity of heat removal from the radiator fins to the environment. When the number of operating fans is reduced from three to one, the average air velocity in the radiator zone drops, leading to a proportional decrease in convective energy transfer.

According to the Newton-Richman law of convective heat transfer, which is a specific case of implementing boundary conditions for equation (3), the dissipated thermal power Q can be expressed as [23]:

$$Q = \alpha \cdot A \cdot (T_{rad} - T_{amb}) \quad (7)$$

Table 9: Temperature values at different system points at various numbers of working fans

Number of fans, pcs.	Temperature, K, at system point					
	CPU enter	**CPU exit**	**GPU enter**	**GPU exit**	**Radiator enter**	**Radiator exit**
3	325.8	326.4	324.9	325.8	326.4	325.0
2	331.2	331.9	330.4	331.3	331.8	330.5
1	352.5	353.2	351.8	352.6	353.1	351.8

where α is the heat transfer coefficient, which depends on the flow velocity ($\alpha \sim u^n$). When using only one fan, the coefficient α decreases significantly due to the reduction in $\mathbf{u}$. To maintain the removal of the total thermal power of the system ($Q \approx 600$ W), the system is forced to increase the temperature gradient ($T_{rad} - T_{amb}$).
Substituting the values obtained during the simulation, it can be observed that with three fans operating, the system maintains a stable mode [11]; however, when switching to one fan, the temperature gradient ∇T in equation (3) is forced to increase. This is confirmed by the temperature rise of the most loaded element (GPU) from 337.4 K to 362.4 K:

$$\Delta T_{total} = T_{1_fan} - T_{3_fans} = 362.4 - 337.4 = 25\,\mathrm{K} \tag{8}$$

Such a 7.4 percent (or 25 K) temperature increase indicates that at low velocity $\mathbf{u}$, the diffusive heat transfer in the air cannot compensate for the lack of forced convection, leading to thermal saturation of the radiator and taking the system beyond safe operating limits. Thus, the calculation confirms that for high-power technical configurations, the presence of three fans is not redundant but a necessary condition to ensure the required value of the velocity vector $\mathbf{u}$ within the framework of equation (1).

5.4 Analysis of hydrodynamic characteristics and pressure distribution

The physical interpretation of the pump unit's operation and the refrigerant's movement in the system is based on the combined solution of equations (1) and (4). The Navier-Stokes equation (1) describes the balance of forces acting on an elementary volume of liquid. In the context of this model, the dominant factor is the pressure gradient ∇p created by the pump to overcome the forces of viscous friction $\mu \nabla^2 \mathbf{u}$.
The total energy of a fluid consists of static pressure and dynamic head. The pump's function is to provide the liquid with excess static pressure, which reaches a maximum value of $P_{max} \approx$ 50912 Pa at the reservoir outlet (Fig. 5). This pressure is consumed to overcome the hydraulic resistance in the microchannels of the CPU and GPU water blocks.
By substituting the values of flow velocity $\mathbf{u}$ and density ρ into equation (4), the dynamic head can be estimated:

$$P_{dyn} = \frac{\rho |\mathbf{u}|^2}{2} \tag{9}$$

At an average flow velocity in the tubes of $\mathbf{u} \approx 1.5$ m/s and a water density of $\rho \approx 1000$ kg/m$^\mathbf{3}$, the dynamic pressure is approximately 1125 Pa. Comparing this value with the total

pressure drop in the system shows that the main part of the pump's energy is spent not on accelerating the flow, but on overcoming resistance (Δp_{loss}) in the narrow sections of the water blocks, which is mathematically described by the second term on the right side of equation (1). Thus, the visualization of velocity vectors in Figure 8 confirms that in areas of sharp channel narrowing, the potential pressure energy is converted into kinetic energy of the flow, which intensifies the heat transfer previously described by equation (3).

6 Conclusion

During the study, a comprehensive evaluation of the efficiency of a liquid cooling system for high-power elements of technical means was carried out using a 3D modeling environment and the FloEFD calculation module. The obtained results confirm that the system is capable of operating at ambient temperatures ranging from 263 K to 313 K. However, at an ambient temperature of 313 K, the system reaches critical temperatures: the central processing unit heats up to 352.0 K, and the graphics processing unit reaches 355.9 K, which may lead to increased component wear.

The analysis of the refrigerant type showed that distilled water demonstrates the best thermophysical characteristics. Its use allows maintaining the CPU temperature at 332.3 K, which is 15.6 K more effective compared to EK-CryoFuel freon (347.9 K) and 11.5 K more effective than Koolance LIQ-702 freon (343.8 K). Furthermore, systems using distilled water are more accessible and easier to maintain.

The configuration of the radiator fan system critically affects operational stability. Calculations proved that a three-section cooling system decreases temperature indicators on average by 25 K (9 percent) compared to using only a single fan. The use of a two-section cooling system is also acceptable, providing a temperature decrease of approximately 19 K (6 percent). At the same time, operating this configuration with only one working fan is unacceptable, as temperatures increase significantly to approximately 362 K, which may quickly lead to system failure.

Based on the above, it can be stated that liquid cooling systems are quite complex in preparation and component selection. However, this drawback is fully compensated by the low temperatures of its components, which increases their efficiency and extends their service life.

References

[1] Piskun, G. A. Simulation of thermal energy removal from processors using air coolers / G. A. Piskun [et al.] // Doklady BGUIR. – 2023. – Vol. 21, No. 4. – P. 54–62. https://doi.org/10.35596/1729-7648-2023-21-4-54-62

[2] Piskun G. A., Alekseev V. F., Stsepchankou A. V., Popov A. N., Belikov A. N., Rybakov D. G. Effect of the configuration and shape of external ribs of sealed enclosures of electronic devices on heat removal efficiency // Journal of the Russian Universities. Radioelectronics. — 2023. — Vol. 26, No. 5. — P. 63–75. https://doi.org/10.32603/1993-8985-2023-26-5-63-75.

[3] Piskun G. A., Alekseev V. F., Stsepchankou A. V., Popov A. N., Belikov A. N., Rybakov D. G. Assessment of the influence of the length and number of heat pipes on the efficiency of the removal of excess thermal energy from the processor // Proceedings of the National Academy of Sciences of Belarus. Physical-Technical Series. — 2024. — Vol. 69, No. 2. — P. 139–150. https://doi.org/10.29235/1561-8358-2024-69-2-139-150

[4] Intel Core i9-13900K. Date of the Last Access (2025, March 29). Retrieved from: `https://www.intel.com`.

[5] EK-CPU Lignum – Walnut. Date of the Last Access (2025, March 29). Retrieved from: `https://www.ekwb.com`.

[6] GeForce RTX 3090 Founders Edition. Retrieved from: `https://www.ixbt.com/3dv/nvidia-geforce-rtx-3090-review.html`.

[7] EK-Quantum Vector FE RTX 3090 D-RGB – Black Special Edition. Date of the Last Access (2025, March 29). Retrieved from: `https://www.ekwb.com/shop/ek-quantum-vector-fe-rtx-3090-d-rgb-black-special-edition`.

[8] EK-CoolStream Classic PE 360. Date of the Last Access (2025, March 29). Retrieved from: `https://www.ekwb.com`.

[9] Corsair AF120 SLIM. Date of the Last Access (2025, March 29). Retrieved from: `https://www.corsair.com`.

[10] EK-Quantum Kinetic³ FLT 92 D5 PWM D-RGB – Plexi. Date of the Last Access (2025, March 29). Retrieved from: `https://www.ekwb.com`.

[11] Nasibullaev I. Sh., Darintsev O. V. Computer 2D modelling of a micro-grip fluid cooling system // Computational Technologies. — 2021. — Vol. 26, No. 2. — P. 4–20. DOI: 10.25743/ICT.2021.26.2.002.

[12] Landsberg G. S. Elementary textbook of physics. Vol. 1. Mechanics. Heat and molecular physics. — Moscow: RIPOL Classic, 2013. — 624 p.

[13] Akhremenkov A. A., Tsirlin A. M. Mathematical model of liquid immersion cooling system for supercomputer // Program Systems: Theory and Applications. — 2016. — Vol. 7, No. 1. — P. 187–199.

[14] Piskun, G. A. Influence of the channels orientation in air coolers on the efficiency of heat removal from processors / G. A. Piskun [et al.] // Doklady BGUIR. – 2023. – Vol. 21, No. 5. – P. 33–41. https://doi.org/10.35596/1729-7648-2023-21-5-33-41

[15] Ihsan Ali Ghani. Heat transfer enhancement in microchannel heat sink using hybrid technique of ribs and secondary channels / Ihsan Ali Ghani [et al.] // International Journal of Heat and Mass Transfer. – 2017. – Vol. 114. – P. 640–655. https://doi.org/10.1016/j.ijheatmasstransfer.2017.06.103

[16] Chenyang Yu. Optimization of elliptical pin-fin microchannel heat sink based on artificial neural network / Chenyang Yu [et al.] // International Journal of Heat and Mass Transfer. – 2023. – Vol. 205. – Art. 123928.. https://doi.org/10.1016/j.ijheatmasstransfer.2023.123928

[17] Abed, A. M. Applications of hybrid nanofluids in microchannel heat sinks: a comprehensive review / A. M. Abed [et al.] // Journal of Thermal Analysis and Calorimetry. – 2025. – Vol. 150. – P. 15883–15901. https://doi.org/10.1007/s10973-025-14626-6

[18] Vilarrubi, M. Experimental and numerical study of micro-pin-fin heat sinks with variable density for increased temperature uniformity / M. Vilarrubi [et al.] // International Journal of Thermal Sciences. – 2018. – Vol. 132. – P. 424–434. https://doi.org/10.1016/j.ijthermalsci.2018.06.019

[19] Wilcox D. C. Turbulence modeling for CFD. — 3rd ed. — La Canada: DCW Industries, 2006. — 522 p.

[20] Launder B. E., Spalding D. B. Lectures in mathematical models of turbulence. — London; New York: Academic Press, 1972. — 169 p.

[21] Bird R. B., Stewart W. E., Lightfoot E. N. Transport phenomena. — 2nd ed. — New York: Wiley, 2002. — 912 p.

[22] Patankar S. V. Numerical heat transfer and fluid flow. — New York: McGraw-Hill, 1980. — 214 p.

[23] Isachenko V. P., Osipova V. A., Sukomel A. S. Heat transfer. — Moscow: Mir Publishers, 1977. — 490 p.

[24] Samarskii A. A. The theory of difference schemes. — Moscow: Nauka, 1977. — 656 p. (in Russian).

[25] Dulnev G. N. Heat and mass transfer in radio-electronic equipment. — Moscow: Vysshaya shkola, 1984. — 247 p.

[26] Kondratyev G. M. Regular thermal regime. — Moscow: Gostekhteoretizdat, 1954. — 408 p.

[27] Kutateladze S. S. Fundamentals of heat transfer. — Moscow: Atomizdat, 1979. — 416 p. (in Russian).

[28] Loitsyanskii L. G. Mechanics of liquids and gases. — Moscow: Drofa, 2003. — 840 p. (in Russian).

G.A. Piskun,
Belarusian State University of Informatics and Radioelectronics,
Petrusia Brovka Street, 6,
Email: piskunbsuir@gmail.com,

V.F. Alekseev,
Belarusian State University of Informatics and Radioelectronics,
Petrusia Brovka Street, 6,
Email: alexvikt.dist@gmail.com

N.A. Pavlavets,
Belarusian State University of Informatics and Radioelectronics,
Petrusia Brovka Street, 6,
Email: nikita.pawlavets@gmail.com

Received 06.05.2025, Revised 15.12.2025, Accepted 08.01.2026, Available online 31.03.2026.